Canadian Geotechnical Journal, Vol. 50, No. 4, pp. 400-412, 2013

Cyclic tests on high-quality undisturbed block samples of soft marine Norwegian clay

T. Wichtmann[i)], K.H. Andersen[ii)], M.A. Sjursen[iii)], T. Berre[iv)]

Abstract: The results of a study with undrained cyclic triaxial and DSS tests on high-quality undisturbed samples obtained from large blocks of a soft marine Norwegian clay are presented. Several tests with different average shear stresses, shear stress amplitudes, loading frequencies and sample geometries have been performed on block samples taken from different depths. In tests with small average shear stresses failure occurred due to large shear strain amplitudes while large permanent shear strains were observed in tests with higher average shear stresses. Diagrams quantifying the undrained cyclic strength, permanent shear strain, shear strain amplitude and permanent pore water pressure in dependence of average shear stress, shear stress amplitude and number of cycles have been developed based on the test results. The undrained cyclic strength was found strongly dependent on loading frequency. Block samples from shallower depth showed a somewhat higher undrained cyclic strength. No influence of the height-to-diameter ratio of the samples ($h/d = 1$ and 2 were compared) could be found. A qualitative comparison of the test results with data for standard tube samples is provided.

Keywords: soft marine clay; block samples; undrained cyclic triaxial tests; undrained cyclic DSS tests

1 Introduction

The foundation design of offshore installations (gravity platforms, piled installations, suction anchors, wind turbines) or structures along the coast (harbours, breakwaters, storm-surge barriers) is governed by the bearing capacity and the serviceability under cyclic loading [3]. The cyclic loading leads to the generation of excess pore water pressure and thus to a deterioration of bearing capacity and soil stiffness. A similar deterioration may occur in the case of on-shore foundations where the cyclic loading is caused by wind (wind turbines), traffic (roads, railway embankments) or earthquake shaking.

Laboratory tests for the determination of cyclic soil parameters are usually performed on tube samples. A comprehensive parametric study with cyclic tests on tube samples of plastic Drammen clay has been documented e.g. in [5] and [2, 3]. In monotonic tests several researchers (e.g. [8, 11, 17]) found a higher shear strength and stiffness for block samples obtained with the Sherbrooke block sampler [14,15] than for standard tube samples. The higher strength and stiffness are due to the lower disturbance of the block samples induced during sampling. Piston samplers with larger diameters, sharp edges and high quality stainless steel tubes can achieve similar results to block samplers. This has been demonstrated e.g. by Hight et al. [11] who compared samples obtained with the Sherbrooke and the Laval [13] sampler.

Cyclic test data on block samples are rare. A comparison of the cyclic behaviour of block and tube samples of silty Drammen clay has been undertaken by Lunne et al. [16]. Three pairs of cyclic triaxial and two pairs of DSS tests were performed. For similar average and cyclic shear stresses, the number of cycles to failure measured for the block samples was twice larger than that obtained for the tube samples.

The experimental study documented in the present paper has been performed in order to collect more cyclic test data on high-quality block samples and to compare these data with data available for standard tube samples. The influences of average shear stress, shear stress amplitude, loading frequency, sampling depth and sample geometry have been studied on block samples of Onsøy clay, a soft marine Norwegian clay.

The data of the present study can be used for feasibility studies and for preliminary design calculations. It may be helpful for setting up laboratory testing programs and for interpreting the data for soils from actual sites.

2 Tested material and testing procedure

The block samples of Onsøy clay used in the present study have been taken approx. 100 km southeast of Oslo close to the city of Fredrikstad. The test site and the basic soil properties have been described by Lunne et al. [17]: The test field lies in an almost flat area with the water table very near to the ground surface. The deposit consists of a weathered crust less than 1 m thick underlain by 8 m of soft clay with iron spots, organic matter and shell fragments and by 36 m of homogeneous soft medium-plastic clay over bedrock. The preconsolidation stresses obtained from constant rate of strain oedometer tests on block samples indicate an OCR decreasing from 1.9 to 1.4 between 7 and 15 m [17]. The average sensitivity as measured by the fall cone test is about 4.5 - 6.0. The salt content of the pore water has been determined as 32.5 g/l.

The block samples of 25 cm diameter were taken using the Sherbrooke block sampler. Three blocks were used for the present study:

- Block No. 18 (height 19 cm) was obtained from a depth 6.93 to 7.12 m below ground. 10 samples for triaxial

[i)] Researcher, Institute of Soil Mechanics and Rock Mechanics (IBF), Karlsruhe Institute of Technology (KIT), Germany (corresponding author). Email: torsten.wichtmann@kit.edu

[ii)] Norwegian Geotechnical Institute (NGI), Sognsveien 72, 0855 Oslo, Norway

[iii)] NGI, Sognsveien 72, 0855 Oslo, Norway

[iv)] NGI, Sognsveien 72, 0855 Oslo, Norway

tests (diameter $d = 54$ mm, height $h = 108$ mm) were cut from this block.

- Block No. 26 (height 40 cm) was taken from a depth 10.50 to 10.90 m below ground. This block was divided into four layers denoted 26A to 26D. 18 samples for triaxial tests ($d = 54$ mm, $h = 108$ mm) were obtained from the upper two layers 26A and 26B. The third layer 26C was used for oedometric compression tests [7]. Five triaxial test samples with a height-to-diameter-ratio of 1 ($d = h = 54$ mm) were cut from the fourth layer 26D.

- Block No. 27 (height 23 cm) was taken from a depth 11.14 to 11.37 m below ground. This block was divided into two layers. 10 triaxial samples ($d = 54$ mm, $h = 108$ mm) were obtained from the upper layer 27A. Three samples for DSS testing ($d = 67$ mm, $h = 16$ mm) were taken from the lower layer 27B.

The individual samples were cut from the blocks keeping at least 3 cm distance to its disturbed boundary. A wire saw was used for cutting.

Liquid limit w_L, plastic limit w_P and plasticity index $I_P = w_L - w_P$ were determined as follows:

- Block No. 18: $w_L = 55.8$ %, $w_P = 29.0$ %, $I_P = 26.8$ %
- Block No. 26: $w_L = 63.0$ %, $w_P = 29.3$ %, $I_P = 33.7$ %
- Block No. 27: $w_L = 62.9$ %, $w_P = 32.6$ %, $I_P = 32.6$ %

Most triaxial tests were performed on samples with a height-to-diameter ratio of 2 ($d = 54$ mm, $h = 108$ mm) and rough end plates, i.e. with filter disks having the same diameter as the sample. A smaller number of tests was performed on samples with a height-to-diameter ratio of 1 ($d = h = 54$ mm). In the latter case stainless steel end plates with a diameter (62 mm) larger than the sample diameter were used. These end plates had a small central porous stone (diameter 5 mm). The end plates were smeared with silicone grease. A latex membrane with a thickness of approx. 0.3 mm was put on top of the grease layer.

All samples were mounted in the triaxial cell with dry filter disks. After the application of a small cell pressure the filter disks and the drainage tubes were flushed with water having the same salt content as the pore water of the samples. After that the samples were re-consolidated under an isotropic stress $\sigma'_{ac} = \sigma'_{rc}$ with effective radial stress σ'_{rc} identical to the in-situ effective horizontal stress σ'_h. The in-situ value of the coefficient of earth pressure at rest $K_0 = 0.6$ was estimated from the correlation of Brooker & Ireland [9]. The isotropic re-consolidation took less than one day. Next, the cell pressure and the back pressure were stepwise increased until a back pressure of 600 kPa was reached. Then, the axial stress was stepwise increased to a σ'_{ac}-value being identical to the in-situ effective vertical stress σ'_v. The in-situ stresses lie between $\sigma'_v = 48.1$ kPa and $\sigma'_h = 28.8$ kPa for block No. 18 and $\sigma'_v = 72.1$ kPa and $\sigma'_h = 43.3$ kPa for the bottom layer of block No. 27 (see Tables 1 and 2 with the monotonic and cyclic testing program, respectively). The samples stood under these anisotropic consolidation stresses over night. Then the saturation was checked by Skempton's B-value. B-values larger than 99 % were reached for all samples. Finally, either a monotonic or a cyclic undrained test was performed.

In all tests the same reconsolidation path has been applied, i.e. an isotropic increase of stress to $\sigma'_a = \sigma'_r = \sigma'_h$ was followed by an increase of axial stress to $\sigma'_a = \sigma'_v$. Hight et al. [11] have demonstrated that the reconsolidation path applied to a clay sample affects its response to undrained shearing. In particular, a higher small-strain stiffness was observed in [11] if the reconsolidation path involved a swelling loop. In the present test series the influence of the reconsolidation path has not been studied. No swelling loop has been applied. The reconsolidation path used in the present test series corresponds to "path B" tested by Hight et al. [11]. In [11] it has been demonstrated that the reconsolidation to in situ effective stresses and the accompanying volumetric strains do not impose further damage to the samples.

The undrained response of clay samples may also be altered by drained creep prior to undrained shearing (e.g. [12]). In the present study all samples stood under their in-situ effective stresses ($\sigma'_a = \sigma'_v$ and $\sigma'_r = \sigma'_h$) over night, i.e. all samples were subjected to a creep phase of similar duration. The effect of a shorter or longer drained creep phase has not been studied in the present test series.

In the cyclic tests the cyclic axial loading was applied load-controlled using a pneumatic loading system. In most tests a loading frequency of 0.1 Hz was used which is representative for wave loading. In one test series the loading frequency was varied between 0.001 Hz and 0.5 Hz.

In some tests, after re-consolidation to the in-situ effective stresses, the drainage was closed and the cyclic loading was applied with an initial average shear stress $t_{a,i}$ being identical to the consolidation shear stress $t_c = (\sigma'_{ac} - \sigma'_{rc})/2$. For example, sample No. 1 (see Table 2) was re-consolidated to $\sigma'_{ac} = 68.1$ kPa and $\sigma'_{rc} = 40.9$ kPa, corresponding to a consolidation shear stress of $t_c = 13.6$ kPa. In that test the cyclic loading was started at an initial average shear stress $t_{a,i} = 13.6$ kPa being identical to the consolidation shear stress. The first cycles were applied with an axial stress amplitude of $\sigma'_{a,cy,i} = 14.0$ kPa, i.e. with a shear stress amplitude $t_{cy,i} = 7.0$ kPa. During a cycle the shear stress therefore varied between $t_{a,i} - t_{cy,i} = 6.6$ kPa and $t_{a,i} + t_{cy,i} = 20.6$ kPa. During a load-controlled cyclic test, due to changes of the sample cross section and due to membrane effects, the average shear stress t_a and the shear stress amplitude t_{cy} may change. A discussion on how these changes are considered in the analysis of the test data is provided in Section 4.

In other tests, after closure of drainage, the total axial stress was increased or decreased in order to reach a shear stress $t_{a,i} \neq t_c$. After a resting period of approx. 2 hours the cyclic loading was started at $t_{a,i}$. For example, sample No. 14 was re-consolidated to $\sigma'_{ac} = 68.8$ kPa and $\sigma'_{rc} = 41.4$ kPa, corresponding to $t_c = 13.7$ kPa. After closure of drainage, the axial load was reduced to isotropic conditions (i.e. $\sigma'_a = 41.4$ kPa, $t = 0$ kPa). The cyclic loading was then started with an average shear stress $t_{a,i} = 0$ kPa.

The pore water pressure was measured at the lower end plate. No mid-plane pore water pressure measurements were performed. The axial strain rate chosen in the monotonic tests is small enough in order to guarantee a homogeneous pore water distribution in the sample. In the cyclic tests, in particular in the case of large amplitudes and high loading frequencies, the pore water pressure measurements

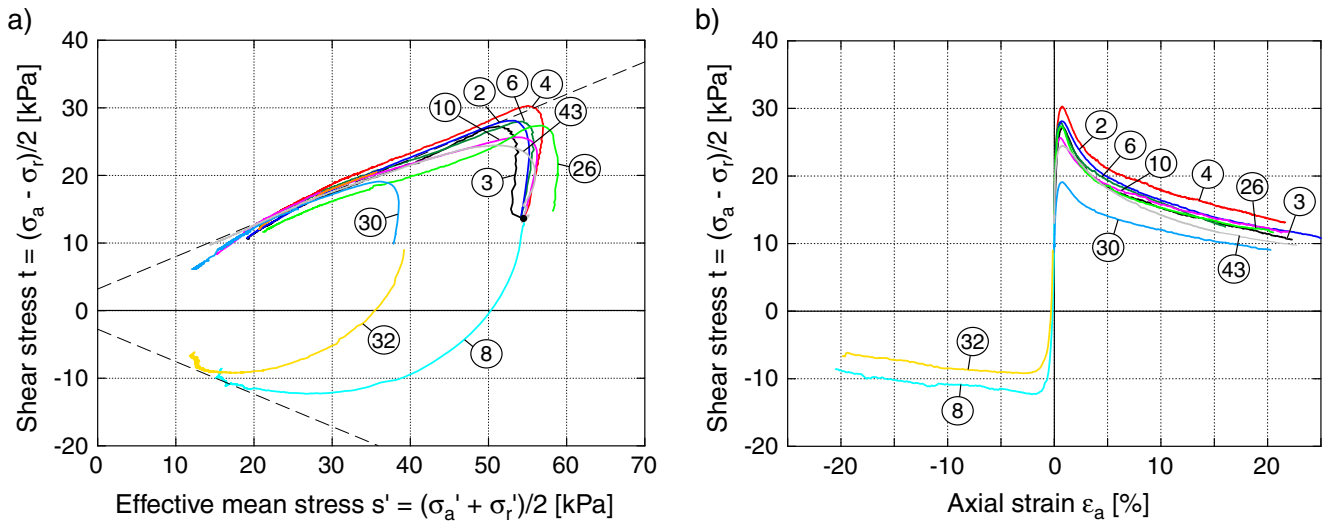

Fig. 1: *Results of undrained monotonic triaxial tests: a) t-s′ effective stress paths, b) shear stress t versus axial strain ε_a*

Sample No	Block Layer	Position in block	h/d [-]	Triaxial cell	Filter papers	comp./ ext.	σ'_{ac} [kPa]	σ'_{rc} [kPa]	t_c [kPa]	w_c [%]	$\varepsilon_{vol,c}$ [%]	$\Delta e_c/e_0$ [-]	s_u [kPa]
3	26A	peripheral	2	monotonic	without	comp.	68.1	40.9	13.6	62.5	1.4	0.017	27.3
4	26A	central	2	cyclic	with	comp.	68.1	40.9	13.6	63.1	1.7	0.023	30.3
6	26A	peripheral	2	cyclic	without	comp.	68.1	40.9	13.6	64.0	1.6	0.022	28.0
2	26A	central	2	cyclic	without	comp.	68.1	40.9	13.6	62.6	1.5	0.023	28.1
10	26A	peripheral	2	cyclic	with	comp.	68.1	40.9	13.6	63.4	-	-	25.6
8	26A	peripheral	2	cyclic	without	ext.	68.1	40.9	13.6	62.6	1.7	0.028	-12.3
26	27A	peripheral	2	cyclic	without	comp.	71.6	43.0	14.3	67.5	2.0	0.026	27.4
30	18	peripheral	2	cyclic	without	comp.	48.1	28.8	9.7	67.9	1.7	0.026	19.1
32	18	peripheral	2	cyclic	without	ext.	48.1	28.8	9.7	65.8	1.6	0.027	-9.2
43	26D	peripheral	1	cyclic	without	comp.	69.5	41.7	13.9	65.1	2.4	0.038	24.4

Table 1: Program of monotonic triaxial tests (all tests: shearing rate $\dot{\varepsilon}_a = 1.4$ %/h).

may not be fully reliable. Only the permanent excess pore water pressure at the end of a cycle u_p, measured at $t = t_a$, is discussed in the present paper. An inspection of the permanent pore pressure has been undertaken on a sample (No. 1 in Table 2) which did not fail after 30,000 cycles applied with a shear stress amplitude $t_{cy} = 7$ kPa and a loading frequency of 0.1 Hz. In that test, the permanent excess pore pressure during the last few cycles was $u_p = 14.4$ kPa. The cyclic loading was stopped and a resting period of 30 minutes followed, allowing for an equalization of the pore water pressure in the sample. The excess pore water pressure at the end of this resting period was $u = 15.9$ kPa. After that two packages of 20 or 20,000 cycles were applied with $t_{cy} = 7$ kPa and with frequencies of 0.01 or 0.5 Hz, respectively. Each package was again followed by a resting period of 30 minutes. The permanent values of pore water pressure were $u_p = 15.8$ or 14.6 kPa for 0.01 or 0.5 Hz, respectively, while an excess pore pressure of 15.9 kPa was retrieved at the end of each resting period. In the following, the data from the cyclic tests are primarily discussed in terms of shear stress and strains. The diagrams given for the permanent pore water pressure should be applied with care since they are affected by measurement errors, as demonstrated by the preliminary tests on sample No. 1.

The void ratio change $\Delta e_c/e_0$ during re-consolidation to the in-situ effective stresses was taken as a criterion in order to quantify the sample disturbance. According to [17], for clays with OCR-values between 1 and 2, $\Delta e_c/e_0$-values lower than 0.04 mean a very good to excellent sample quality while it is good to fair for $0.04 \leq \Delta e_c/e_0 \leq 0.07$. All samples from the two uppermost layers of block No. 26 (26A: $\Delta e_c/e_0 = 0.017$ - 0.039, 26B: $\Delta e_c/e_0 = 0.023$ - 0.034), from the top layer of block No. 27 (27A: $\Delta e_c/e_0 = 0.021$ - 0.032) and from block No. 18 ($\Delta e_c/e_0 = 0.016$ - 0.027) fall into the category "very good to excellent". The disturbance of the samples with a height-to-diameter ratio of 1 obtained from the bottom of block No. 26 is somewhat higher ($\Delta e_c/e_0 = 0.032$ - 0.065), but the sample quality is still in the category "good to fair".

3 Monotonic triaxial tests

The monotonic triaxial tests were performed in order to determine the undrained shear strength s_u which is used as a reference in the interpretation of the cyclic test data. Five triaxial compression tests (samples Nos. 2, 3, 4, 6 and 10) and one triaxial extension test (sample No. 8) were performed on samples from the first layer of block No. 26 (see the testing program in Table 1). All samples measured $d = 54$ mm in diameter and $h = 108$ mm in height. Two samples (Nos. 2 and 4) were cut from the center of the block, while all other samples (Nos. 3, 6, 8 and 10) were taken from a peripheral position. One test (sample No. 3) was performed with a triaxial cell which is usually applied for monotonic triaxial testing while all other tests were performed with the same triaxial cell which was also used for the cyclic tests. In order to improve drainage, the lateral boundary

Test series	Sample No.	Block Layer	Pos	h /d [-]	σ'_{ac} [kPa]	σ'_{rc} [kPa]	t_c [kPa]	s_u^c [kPa]	$t_{a,i}$ [kPa]	$t_{a,i}$ /s_u^c [-]	$t_{cy,i}$ [kPa]	$t_{cy,i}$ /s_u^c [-]	f [Hz]	w_c [%]	$\varepsilon_{\mathrm{vol},c}$ [%]	Δe_c /e_0 [-]	N_f [-]
1	1	26A	P	2	68.1	40.9	13.6	28.0	13.6	0.49	7.0	0.25	0.1	64.0	1.8	0.028	>30,000
	15	26B	C	2	68.8	41.4	13.7	28.3	13.7	0.48	9.2	0.325	0.1	63.2	1.4	0.023	1362
	9	26A	P	2	68.1	40.9	13.6	28.0	13.6	0.49	11.2	0.40	0.1	62.7	1.5	0.017	759
	25	27A	P	2	71.6	43.0	14.3	27.4	14.3	0.52	11.8	0.43	0.1	67.4	2.0	0.032	169
	5	26A	P	2	68.1	40.9	13.6	28.0	13.6	0.49	15.0	0.54	0.1	63.0	2.3	0.039	37
	7	26A	P	2	68.1	40.9	13.6	28.0	13.6	0.49	19.6	0.70	0.1	63.6	1.8	0.028	13
	28	27A	C	2	71.6	43.0	14.3	27.4	14.3	0.52	19.2	0.70	0.1	67.6	2.1	0.032	10
2	14	26B	P	2	68.8	41.4	13.7	28.3	0	0	7.1	0.25	0.1	60.7	1.7	0.029	>28,000
	12	26B	P	2	68.8	41.4	13.7	28.3	0	0	11.2	0.40	0.1	62.3	1.8	0.023	250
	11	26B	P	2	68.8	41.4	13.7	28.3	0	0	15.6	0.55	0.1	63.0	1.9	0.028	17
3	13	26B	P	2	68.8	41.4	13.7	28.3	7.1	0.25	11.3	0.40	0.1	63.4	2.4	0.034	679
	18	26B	P	2	68.8	41.4	13.7	28.3	7.1	0.25	15.6	0.55	0.1	62.5	1.8	0.029	113
	27	27A	C	2	71.6	43.0	14.3	27.4	6.9	0.25	21.9	0.80	0.1	66.7	2.0	0.032	10
	16	26B	P	2	68.8	41.4	13.7	28.3	21.2	0.75	7.1	0.25	0.1	63.6	1.7	0.028	246
	17	26B	P	2	68.8	41.4	13.7	28.3	-5.7	-0.20	7.1	0.25	0.1	62.7	1.9	0.034	205
4	19	27A	P	2	71.6	43.0	14.3	27.4	14.3	0.52	11.8	0.43	0.5	67.3	1.7	0.021	800
	20	27A	P	2	71.6	43.0	14.3	27.4	14.3	0.52	19.2	0.43	0.01	67.5	1.5	0.021	30
	21	27A	P	2	71.6	43.0	14.3	27.4	14.3	0.52	7.4	0.27	0.01	68.0	1.7	0.026	294
	22	27A	P	2	71.6	43.0	14.3	27.4	14.3	0.52	7.4	0.27	0.001	68.0	1.6	0.021	100
	23	27A	P	2	71.6	43.0	14.3	27.4	0	0	7.4	0.27	0.001	66.8	2.1	0.027	>400
	24	27A	P	2	71.6	43.0	14.3	27.4	0	0	11.8	0.43	0.001	67.0	2.0	0.027	21
5	34	18	P	2	48.1	28.8	9.7	19.1	9.7	0.51	5.7	0.30	0.01	66.2	1.4	0.021	17,511
	29	18	P	2	48.1	28.8	9.7	19.1	9.7	0.51	7.6	0.40	0.01	66.3	1.4	0.021	818
	31	18	P	2	48.1	28.8	9.7	19.1	9.7	0.51	10.5	0.55	0.01	66.7	1.6	0.021	109
	33	18	P	2	48.1	28.8	9.7	19.1	9.7	0.51	13.4	0.70	0.01	66.6	1.6	0.021	21
	36	18	P	2	48.1	28.8	9.7	19.1	9.7	0.51	17.2	0.90	0.01	66.8	1.2	0.016	6
	37	18	C	2	48.1	28.8	9.7	19.1	0	0	5.7	0.30	0.01	67.1	1.4	0.021	7,883
	35	18	P	2	48.1	28.8	9.7	19.1	0	0	7.4	0.55	0.01	66.5	1.4	0.021	29
	38	18	C	2	48.1	28.8	9.7	19.1	0	0	13.4	0.70	0.01	66.2	1.4	0.021	9
6	41	26D	P	1	69.5	41.7	13.9	24.4	13.9	0.57	8.6	0.35	0.01	63.2	2.8	0.044	1195
	40	26D	P	1	69.5	41.7	13.9	24.4	13.9	0.57	11.5	0.47	0.01	62.9	4.5	0.065	62
	42	26D	P	1	69.5	41.7	13.9	24.4	13.9	0.57	11.5	0.47	0.01	65.3	2.1	0.032	69
	39	26D	C	1	69.5	41.7	13.9	24.4	13.9	0.57	15.8	0.65	0.01	65.0	2.8	0.038	17

Table 2: Program of cyclic triaxial tests (Pos = Position in block, C = central, P = peripheral).

of two samples (Nos. 4 and 10) was equipped with strips of filter papers which were inclined by 45°. The other samples were tested without filter paper strips. The shearing was applied with an axial strain rate of $\dot{\varepsilon}_a = 1.4$ %/h in all tests. The t-s' effective stress paths with effective mean pressure $s' = (\sigma'_a + \sigma'_r)/2$ and shear stress $t = (\sigma'_a - \sigma'_r)/2$ are given in Figure 1a while the curves of shear stress versus axial strain ε_a are shown in Figure 1b. The shape of the effective stress paths measured in the present test series is similar to that observed by Lunne et al. [17] in their tests on block samples. The effective stress paths and stress-strain relationships given in Figure 1 do not show an influence of the position of the sample in the block, of the type of triaxial cell applied or whether filter papers are used or not. Therefore, a mean value $s_u^c = 28.0$ kPa from all monotonic tests performed on samples from block No. 26A was used as a reference for the analysis of the cyclic test data collected for samples from block No. 26A. The cyclic test data for block layer 26B were normalized with $s_u^c = 28.3$ kPa, assuming a linear increase of s_u^c with depth. In the triaxial extension test, an undrained shear strength of $s_u^e = 12.3$ kPa was measured, corresponding to a ratio $s_u^e/s_u^c = 0.44$. A similar average value $s_u^e/s_u^c = 0.47$ was obtained by Lunne et al. [17] from three pairs of compression and extension tests on Onsøy clay block samples taken from different depths.

In a triaxial compression test on sample No. 26 from the upper layer of block No. 27 an undrained shear strength of $s_u^c = 27.4$ kPa was measured (Figure 1, Table 1). This s_u^c-value was taken as reference for the analysis of the cyclic tests performed on samples from block layer 27A.

A triaxial compression test on sample No. 30 from block No. 18 showed an undrained shear strength of $s_u^c = 19.1$ kPa while the triaxial extension test (sample No. 32) led to $s_u^e = 9.2$ kPa (Figure 1, Table 1), corresponding to a ratio $s_u^e/s_u^c = 0.48$. The s_u^c-value was used as reference for the cyclic tests on samples from block No. 18.

Finally, a triaxial compression test was performed on a sample with a height-to-diameter-ratio of 1 ($h = d =$ 54 mm). The sample No. 43 taken from the lowest layer of block No. 26 showed larger void ratio changes during reconsolidation than the samples with $h/d = 2$ taken from the first layer of the same block (compare the $\Delta e_c/e_0$ values in Table 1). A comparatively low undrained shear strength of $s_u^c = 24.4$ kPa was obtained (Figure 1, Table 1) for this sample. It was used as a reference for the cyclic tests on samples with $h/d = 1$.

4 Cyclic triaxial tests

All cyclic tests were performed without filter papers at the boundary of the samples in order to prevent a reinforcement effect, especially at large strain amplitudes. Failure was defined when either the single amplitude or the permanent value of axial strain ε_a (i.e. the strain at the end of a cycle) reached 10 % (i.e. shear strain $\gamma = 15$ %). The testing program is summarized in Table 2.

4.1 Influence of average shear stress and shear stress amplitude

In a first test series (Table 2), the influence of the shear stress amplitude was studied at the in-situ average shear

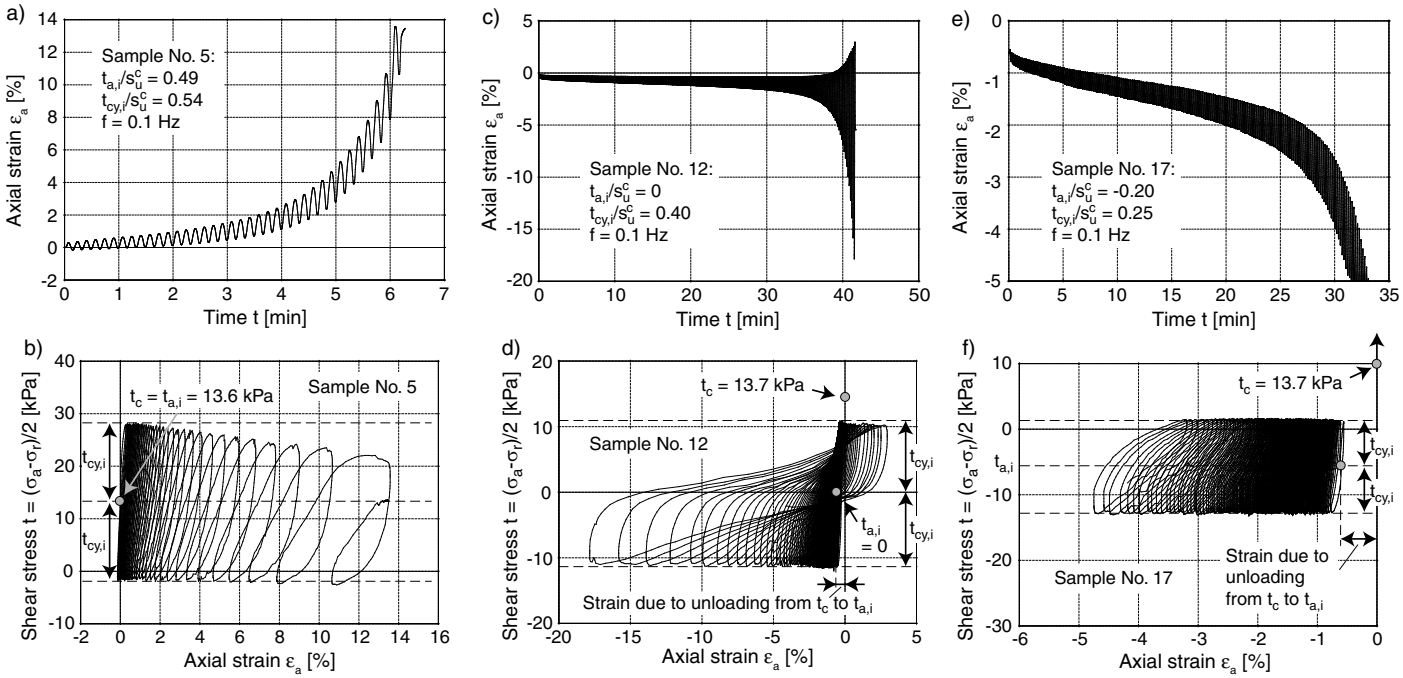

Fig. 2: *Results of cyclic tests on samples Nos. 5, 12 and 17*

stress. The samples were re-consolidated to their in-situ effective stresses and then subjected to an undrained cyclic loading with a frequency of 0.1 Hz. The average shear stress $t_{a,i}$ during the first cycles was thus identical to the in-situ shear stress t_0, corresponding to $t_{a,i}/s_u^c$ values between 0.48 and 0.52. Four of the seven tested samples were taken from the first layer of block No. 26 (samples Nos. 1, 5, 7 and 9), one sample (No. 15) was cut from the second layer of block No. 26 and two more samples (Nos. 25, 28) were obtained from the first layer of block No. 27. Different ratios of shear stress amplitude $t_{cy,i}$ and undrained shear strength s_u^c in the range $0.25 \leq t_{cy,i}/s_u^c \leq 0.70$ were applied in the tests. Figure 2a,b presents a typical test result, i.e. the development of axial strain with time and the t-ε_a-hystereses measured in the test on sample No. 5.

The decrease of average shear stress and shear stress amplitude with increasing number of cycles mentioned in Section 2 is visible in Figure 2b. It is due to both an increase of the sample cross section and rubber membrane correction. During the first cycle of the test on sample No. 5, the average shear stress was $t_{a,i} = t_c = 13.6$ kPa and the shear stress amplitude was $t_{cy,i} = 15.0$ kPa. During the cycle before failure, these values were $t_a = 11.3$ kPa and $t_{cy} = 13.0$ kPa only.

Failure was not achieved in the test on sample No. 1 where 30,000 cycles were applied with $t_{a,i}/s_u^c = 0.25$. Independently of the amplitude, all other samples failed due to an accumulation of 10 % permanent axial strain $\varepsilon_{a,p}$ (i.e. $\gamma_p > 15$ %), while the axial strain amplitude $\varepsilon_{a,cy}$ remained relatively small. This becomes clear from the plot of the minimum, maximum and permanent axial strain versus the number of cycles in Figure 3a and from Figure 3b showing the axial strain amplitude as a function of N. Obviously, the number of cycles to failure N_f decreases with increasing amplitude ratio $t_{cy,i}/s_u^c$. This is also evident from Figure 4a where the number of cycles to failure is given as a function of amplitude ratio t_{cy}/s_u^c. Additionally, curves $t_{cy}/s_u^c(N)$ for certain values of permanent shear strain γ_p have been added in Figure 4a. An analogous presentation of curves $t_{cy}/s_u^c(N)$ for certain values of shear strain amplitude γ_{cy} is given in Figure 4b.

It is not clear how the decrease of t_{cy} occurring in some of the tests (see Figure 2b) should be considered in the diagrams given in Figure 4. On one hand, looking at Figure 4a, large amplitudes cause more "damage" to the material than smaller amplitudes. This may justify the use of the largest amplitudes applied during a test (usually the initial values $t_{cy,i}$). On the other hand, the largest strain accumulation rates are measured near the end of the test (see Figure 2a), i.e. when the amplitudes have already decreased. Therefore, using the reduced amplitude values near failure would be reasonable as well. In the analysis of the present test data a compromise between both alternatives has been made. The t_{cy} values used in the diagrams in Figure 4a,b and similar figures in the following are mean values between the shear stress amplitude $t_{cy,i}$ at $N = 1$ and the shear stress amplitude at the permanent shear strain γ_p under consideration. In a similar manner mean values of average shear stress t_a have been calculated and used in the diagrams.

In a second test series the influence of the shear stress amplitude was studied at isotropic average stresses ($t_{a,i} = 0$, Table 2). The three samples Nos. 11, 12 and 14 were cut from the second layer of block No. 26 and subjected to a cyclic loading with $f = 0.1$ Hz. The amplitude ratios were $t_{cy,i}/s_u^c = 0.25$, 0.40 or 0.55, respectively. Typical results from the test on sample No. 12 are given in Figure 2c,d. The minimum, maximum and permanent values of axial strain are plotted as a function of the number of cycles in Figure 3d, while the strain amplitude is shown in Figure 3e. Sample No. 14 did not fail after 28,000 cycles with $t_{cy,i}/s_u^c = 0.25$. Both other samples failed due to an axial strain amplitude exceeding 10 % (i.e. $\gamma_{cy} > 15$ %). Figure 4c compares the curve $t_{cy}/s_u^c(N_f)$ obtained from this test series with that derived from test series No. 1. For a given amplitude ratio

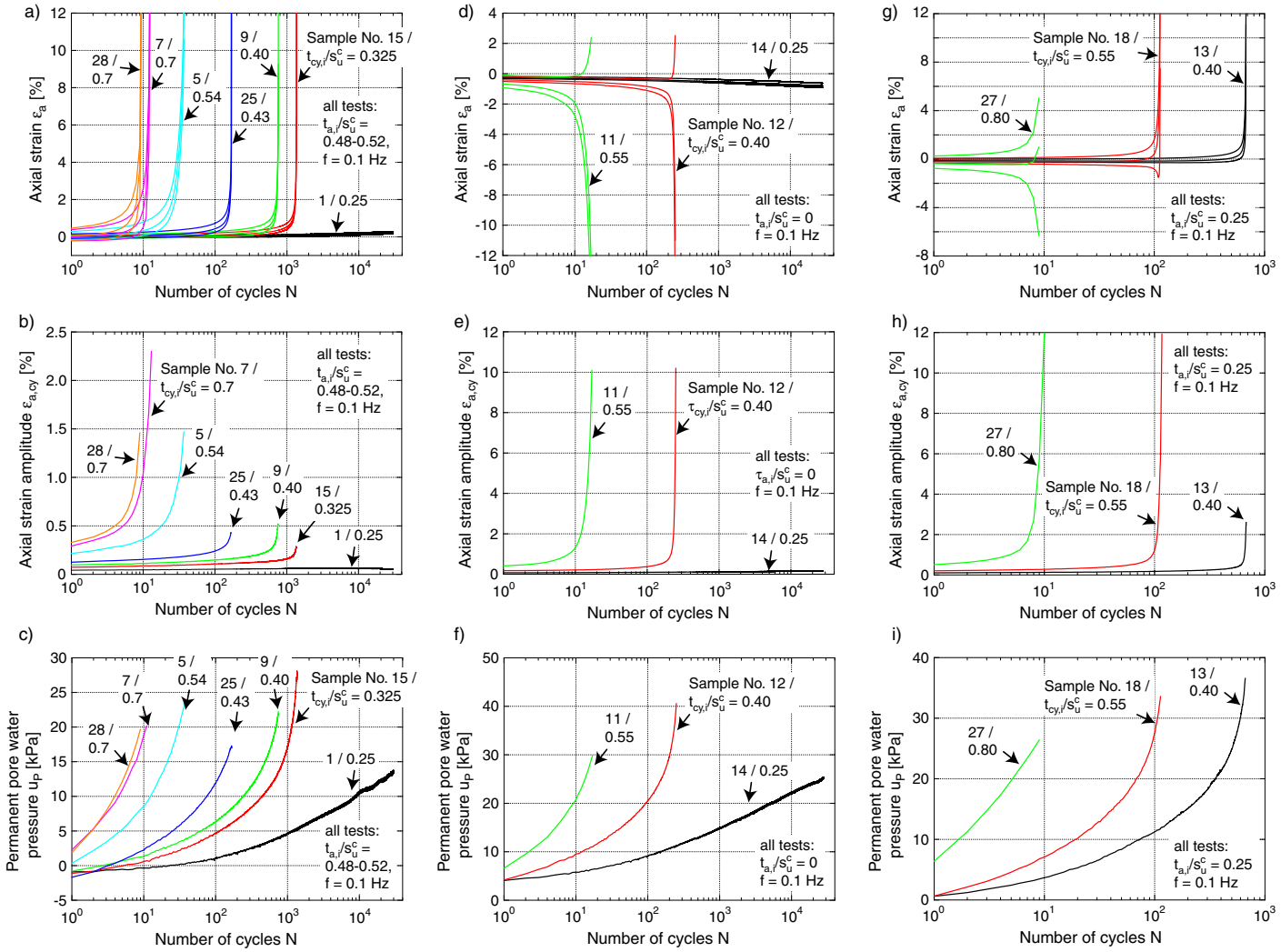

Fig. 3: *Maximum, minimum and permanent axial strain* $\varepsilon_{a,\max}(N)$, $\varepsilon_{a,\min}(N)$ *and* $\varepsilon_{a,p}(N)$ *(first row), strain amplitude* $\varepsilon_{a,cy}(N)$ *(second row) and permanent pore water pressure* $u_p(N)$ *(third row) measured in the tests with a-c)* $t_{a,i}/s_u^c$ = 0.48 - 0.52, *d-f)* $t_{a,i}/s_u^c$ = 0 *and g-i)* $t_{a,i}/s_u^c$ = 0.25

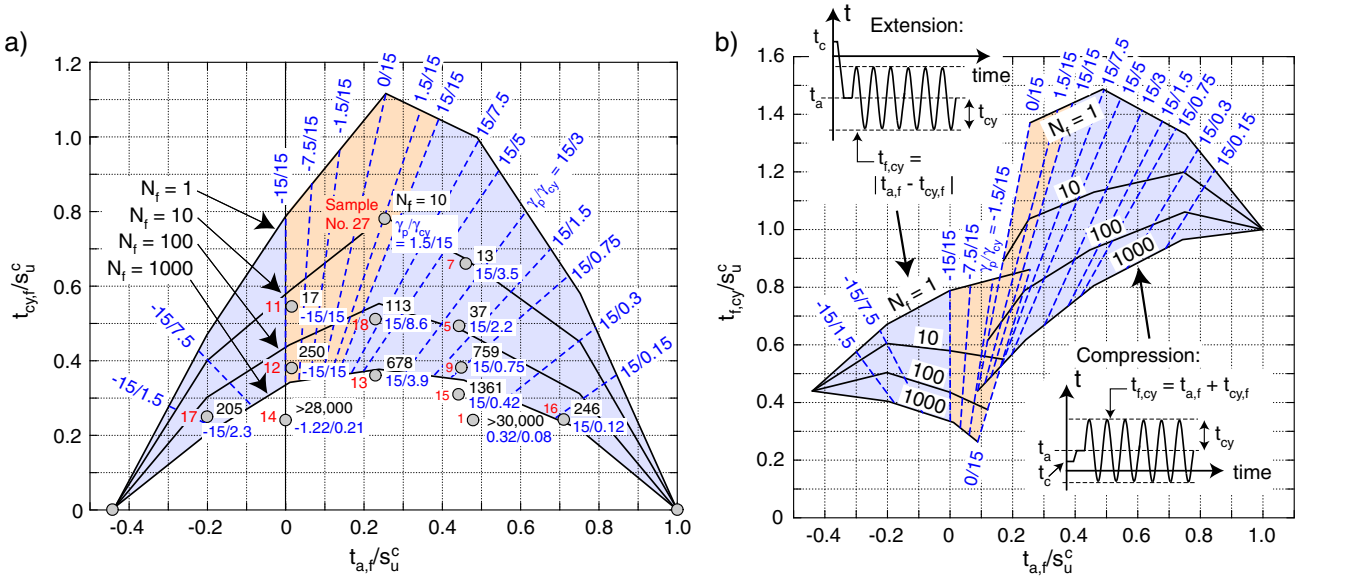

Fig. 5: *a)* t_{cy}/s_u^c-t_a/s_u^c*-diagram with the number of cycles* N_f *to failure and the deformation failure mode* (γ_p, γ_{cy}) *measured for the various tested average shear stresses and shear stress amplitudes. b) Cyclic shear strength ratio* $t_{f,cy}/s_u^c$ *with* $t_{f,cy} = |t_{a,f} - t_{cy,f}|$ *for extension and* $t_{f,cy} = (t_{a,f} + t_{cy,f})$ *for compression as a function of average shear stress ratio* $t_{a,f}/s_u^c$

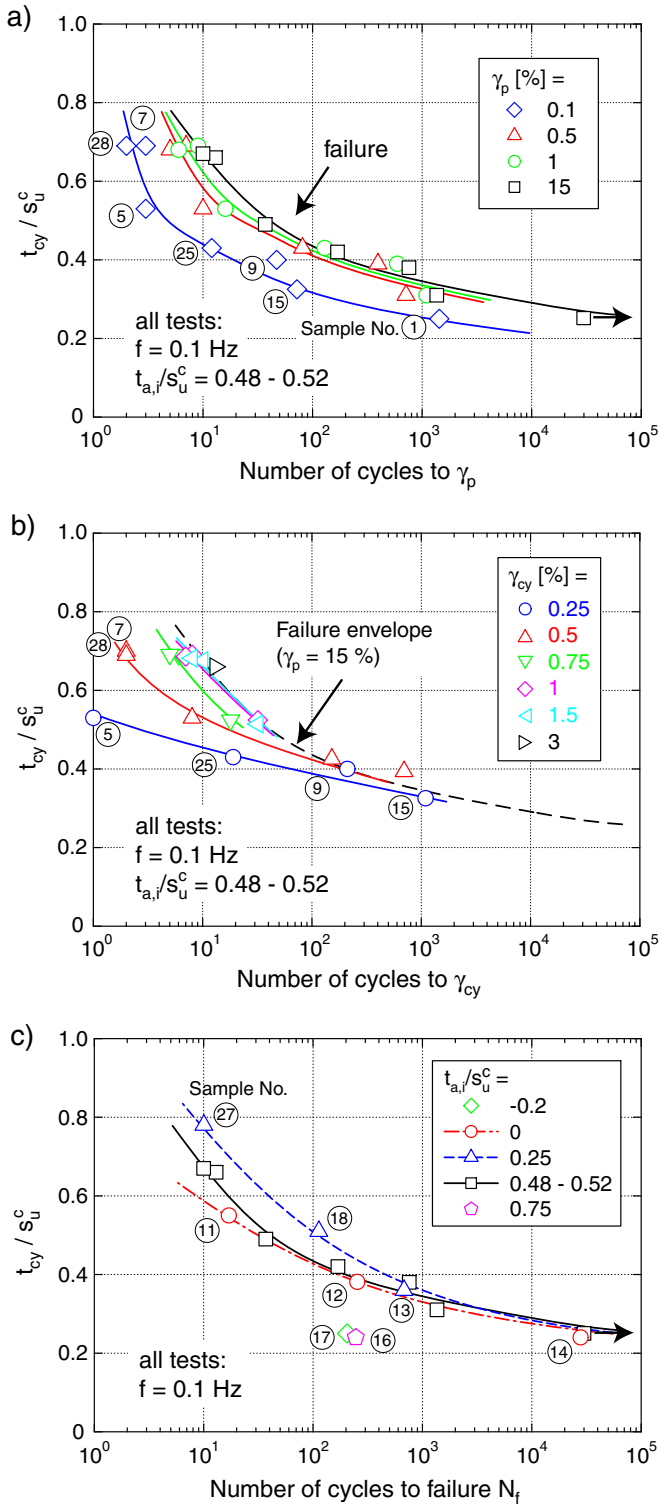

Fig. 4: a) *Curves* $t_{cy}/s_u^c(N)$ *for certain values of permanent shear strain* γ_p *in the tests with* $t_{a,i}/s_u^c$ = 0.48 - 0.52, b) *Curves* $t_{cy}/s_u^c(N)$ *for certain values of shear strain amplitude* γ_{cy} *in the tests with* $t_{a,i}/s_u^c$ = 0.48 - 0.52, c) *comparison of curves* $t_{cy}/s_u^c(N_f)$ *obtained from the three test series with different average shear stress ratios* $t_{a,i}/s_u^c$

t_{cy}/s_u^c, a cyclic loading with $t_{a,i}/s_u^c = 0$ causes failure in a lower number of cycles than a cyclic loading applied at $t_{a,i}/s_u^c$ = 0.48 - 0.52.

Three other average shear stress ratios $t_{a,i}/s_u^c$ = -0.20, 0.25 and 0.75 were tested in a third test series (Table 2). The samples were cut either from the second layer of block No. 26 (samples Nos. 13, 16, 17 and 18) or from the first layer of block No. 27 (sample No. 27). Three different amplitude ratios in the range $0.40 \le t_{cy,i}/s_u^c \le 0.80$ were tested at an average shear stress ratio $t_{a,i}/s_u^c = 0.25$. Figure 3g presents the minimum, average and maximum axial strain versus the number of cycles, while Figure 3h summarizes the corresponding curves of the strain amplitude. The sample tested with the smallest amplitude ratio $t_{cy,i}/s_u^c = 0.40$ failed due to an excessive accumulation of permanent axial strain (Figure 3g). The permanent strain failure mode was also observed for the sample tested with $t_{cy,i}/s_u^c = 0.55$ (Figure 3g), although a significant increase of the strain amplitude was also measured (Figure 3h). In contrast, the largest tested shear stress amplitude $t_{cy,i}/s_u^c = 0.80$ led to failure due to a strain amplitude exceeding $\varepsilon_{a,cy} = 10$ %. Therefore, for an average shear stress ratio $t_{a,i}/s_u^c = 0.25$ the deformation failure mode depends on the shear stress amplitude applied.

The sample tested in the triaxial extension regime ($t_{a,i}/s_u^c$ = -0.20, $t_{cy,i}/s_u^c = 0.25$) failed due to an accumulation of -10 % permanent axial strain (Figure 2e,f). The permanent strain failure mode ($\varepsilon_{a,p} > 10$ %) was also observed in the test with the highest tested average stress ratio $t_{a,i}/s_u^c = 0.75$ and $t_{cy,i}/s_u^c = 0.25$. The numbers of cycles to failure observed in the tests of this series have been added in Figure 4c. Comparing the curves $t_{cy}/s_u^c(N_f)$ for $t_{a,i}/s_u^c$ = 0, 0.25 and 0.48 - 0.52, the highest cyclic resistance is observed for the samples tested at $t_{a,i}/s_u^c = 0.25$.

In Figure 5a the number of cycles to failure N_f is given beside the tested combinations of t_a/s_u^c and t_{cy}/s_u^c in plots of the type proposed by Andersen & Lauritzsen [6]. Isolines for combinations of t_a/s_u^c and t_{cy}/s_u^c causing failure in N_f = 1, 10, 100 and 1000 cycles have been added. The intersection of the isolines with the horizontal axis were assumed equal to 1 and s_u^e/s_u^c = -0.44, based on the undrained shear strength values measured in the monotonic compression or extension tests.

The deformation failure mode (γ_p / γ_{cy}) is also provided in Figure 5a. Isolines for combinations of t_a/s_u^c and t_{cy}/s_u^c showing the same deformation failure mode are given as dashed lines in Figure 5a. A failure due to large strain amplitudes occurs only for average stresses lying between $t_a/s_u^c \approx 0$ and ≈ 0.3. Larger average stress ratios cause failure due to an excessive accumulation of permanent compressive strain, while stress ratios $t_a/s_u^c < 0$ led to failure due to large extensional permanent strains.

The cyclic shear strength $t_{f,cy}$ that can be mobilized during cyclic loading is defined as the sum of the average and cyclic shear stresses at failure. A diagram showing $t_{f,cy}/s_u^c$ as a function of $t_{a,f}/s_u^c$ is given in Figure 5b. The difference between the cyclic strengths in compression and extension is due to the fact that the compression strength is calculated as $t_{f,cy} = (t_{a,f} + t_{cy,f})$ with $t_a \ge 0$, while the extension strength is $t_{f,cy} = |t_{a,f} - t_{cy,f}|$ with $t_a < 0$ (see the schemes in Figure 5b). The diagram in Figure 5b can be used for calculations of the bearing capacity under cyclic loading according to the procedure proposed in [6].

Unfortunately, no cyclic tests on tube samples of Onsøy

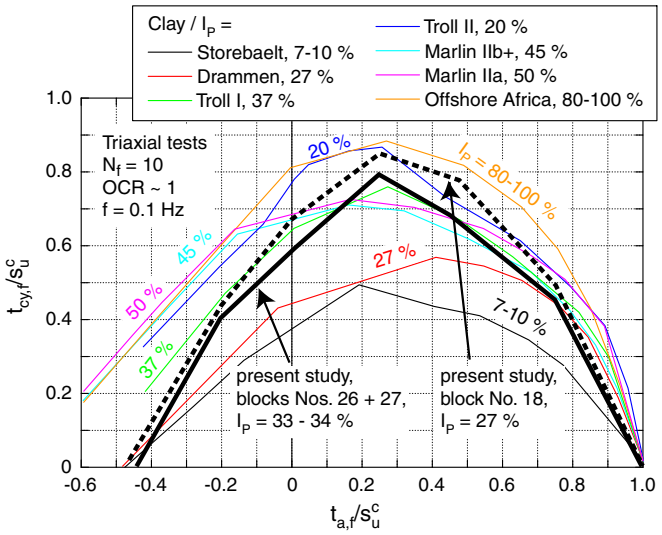

Fig. 6: *Comparison of isolines for $N_f = 10$ obtained from tests on different clays (Figure 27 from [3] supplemented by the test data from the present study)*

clay have been performed so far. Therefore, the potential improvement of the cyclic resistance by using block samples instead of tube samples cannot be quantified yet. However, the results of the present study can be compared with data for tube samples of other soft marine clays. Figure 6 presents isolines for $N_f = 10$ cycles collected by Andersen [2,3] and supplemented by the curve from the present study (blocks 26 and 27). All tested materials are soft offshore marine clays ($OCR = 1$ - 1.5) except Storebælt which is a glacial clay till. With the exception of the present study, all data in Figure 6 were obtained from tests on tube samples. Obviously, despite a significant scatter the cyclic strength increases with increasing plasticity index I_P of the tested material. The isoline from the present study has a similar shape as those from tests on tube samples. In the range $0 \le t_a/s_u^c \le 0.5$, the undrained cyclic strength of the Onsøy clay block samples (I_P = 33 - 34 %) is considerably higher than that of Drammen clay (I_P = 27 %). Despite the lower plasticity index, the cyclic strength of the Onsøy clay block samples is of similar magnitude as that observed for tube samples of Troll I (I_P = 37 %), Marvin IIb+ (I_P = 45 %) and Marvin IIa (I_P = 50 %). It is only slightly lower than that measured for Offshore Africa (I_P = 80 - 100 %). The only exception is Troll II for which a higher undrained cyclic strength than for the Onsøy clay block samples has been measured, despite a lower plasticity (I_P = 20 %).

Figure 7 presents the permanent and cyclic shear strains in diagrams of the type proposed by Andersen & Lauritzsen [5]. For certain numbers of cycles (N = 1, 10 and 100), isolines for combinations of t_a/s_u^c and t_{cy}/s_u^c causing the same values of permanent shear strain γ_p (blue curves) or shear strain amplitude γ_{cy} (red curves), respectively, have been constructed. The test data is given by the numbers close to the tested combinations of t_a/s_u^c and t_{cy}/s_u^c. The intersections of the γ_p-isolines with the horizontal axis have been derived from the t-γ curves measured in the monotonic triaxial compression and extension tests. The diagrams in Figure 7 can be used in order to estimate cyclic or permanent deformations following the procedure proposed in [1] and [4].

The increase of the permanent (excess) pore water pres-

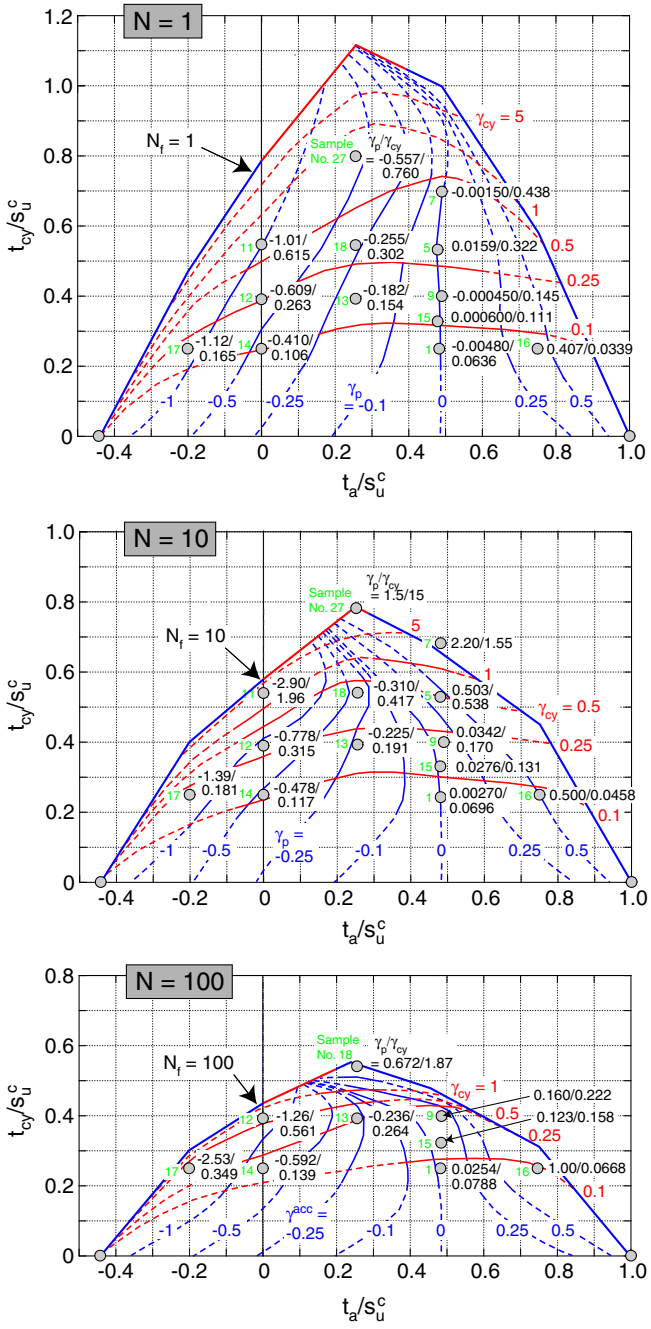

Fig. 7: *Permanent shear strain γ_p and shear strain amplitude γ_{cy} in dependence of average shear stress ratio t_a/s_u^c and shear stress amplitude ratio t_{cy}/s_u^c for N = 1, 10 and 100*

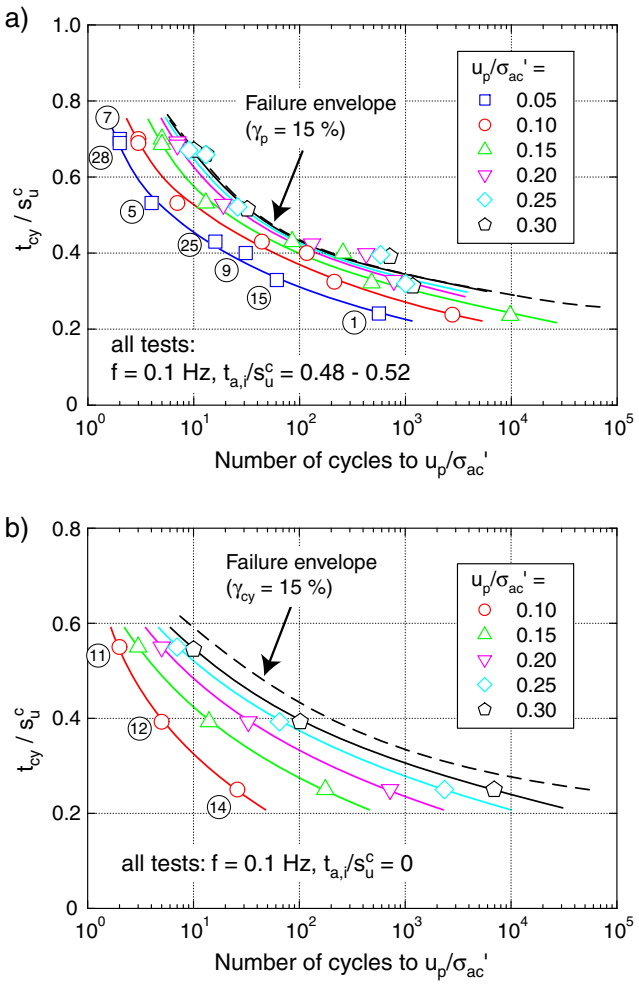

Fig. 8: *Pore pressure ratio u_p/σ'_{ac} in dependence of amplitude ratio t_{cy}/s_u^c and number of cycles for a cyclic loading applied a) at the in-situ average shear stress and b) at $t_{a,i}/s_u^c = 0$*

sure u_p (measured at $t = t_a$) with increasing number of cycles in tests with different average shear stresses and shear stress amplitudes is given in Figure 3c,f,i. The value of the permanent pore pressure u_p does not contain the pore pressure change due to the change $\Delta p = 2/3\Delta t$ of total mean pressure $p = (\sigma_a + 2\sigma_r)/3$ when the average shear stress is changed by Δt from t_c to t_a prior to cyclic loading. Figure 8 shows the permanent pore water pressure ratio u_p/σ'_{ac} with the effective axial consolidation stress σ'_{ac} as a function of amplitude ratio t_{cy}/s_u^c and number of cycles N, based on the test data from the series with $t_{a,i}/s_u^c$ = 0.48 - 0.52 (Figure 8a) and $t_{a,i}/s_u^c = 0$ (Figure 8b). Contour plots of the permanent pore pressure ratio u_p/σ'_{ac} as a function of t_{cy}/s_u^c and t_a/s_u^c for $N = 1$, 10 and 100 are given in Figure 9. The intersections of the isolines with the horizontal axis have been derived from the pore water pressures measured in the monotonic triaxial compression and extension tests. The diagrams in Figures 8 and 9 can be used in order to estimate the settlements associated with the pore pressure dissipation after cyclic loading [18].

4.2 Influence of loading frequency

All cyclic tests presented so far have been performed with a loading frequency of 0.1 Hz. Six other tests have been conducted with frequencies of either 0.001 Hz, 0.01 Hz or 0.5

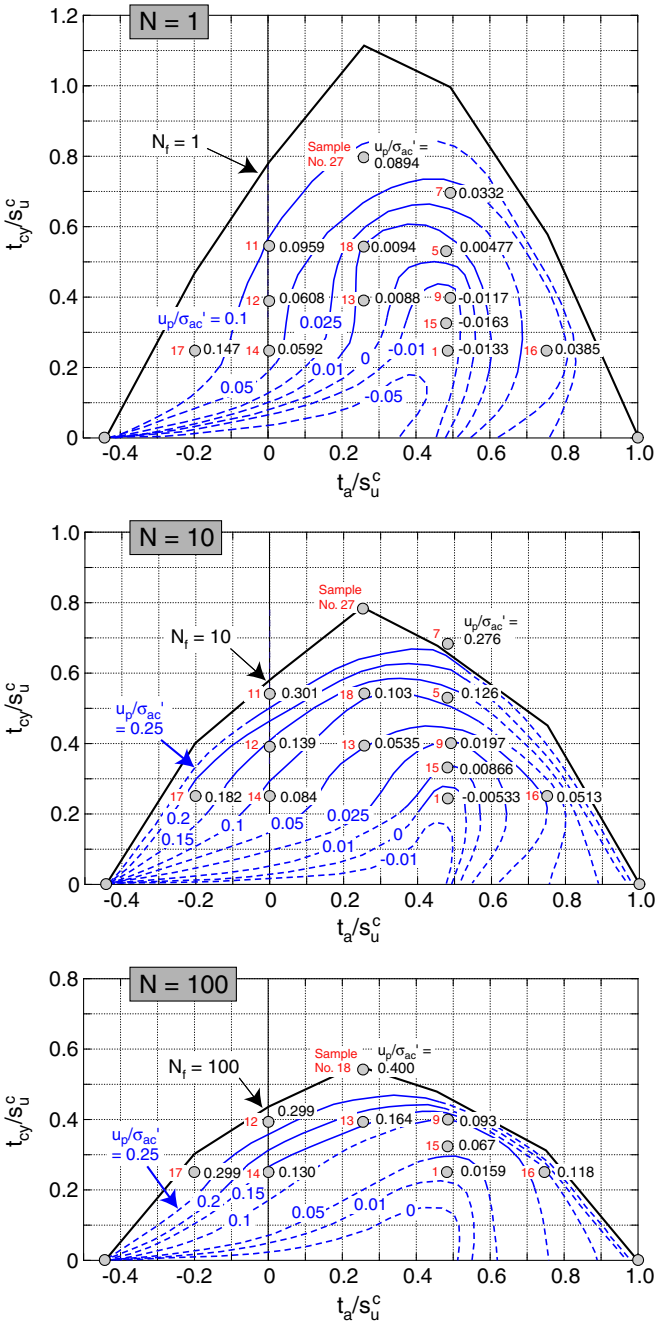

Fig. 9: *Pore pressure ratio u_p/σ'_{ac} in dependence of shear stress amplitude ratio t_{cy}/s_u^c and average shear stress ratio t_a/s_u^c for $N = 1$, 10 and 100*

Hz. All samples were taken from the first layer of block No. 27 (samples Nos. 19 to 24, Table 2). In four tests the cycles were applied at the in-situ average shear stress ($t_{a,i}/s_u^c$ = 0.52). In the two other tests the cyclic loading started at isotropic average stresses ($t_{a,i}/s_u^c = 0$). The test results are summarized in Figure 10. Independently of the frequency, the samples subjected to a cyclic loading with $t_{a,i}/s_u^c$ = 0.52 failed due to an excessive accumulation of permanent strain (Figure 10a), while the strain amplitude remained relatively small (Figure 10b). The samples loaded at $t_{a,i}/s_u^c$ = 0 failed due to an axial strain amplitude exceeding 10 % (Figure 10d,e). The plots of axial strain versus the number of cycles in Figure 10a,d and the t_{cy}/s_u^c-N_f-diagrams in Figure 10c,f reveal that the number of cycles to failure increases with increasing loading frequency. This was observed for both tested average stresses independently of the amplitude. For example, for the samples tested with $t_{a,i}/s_u^c$ = 0.52 and $t_{cy,i}/s_u^c = 0.43$, the cyclic loading with f = 0.01 Hz caused failure in 30 cycles, while 168 cycles (i.e. approx. 6 times more cycles) could be applied in case of a loading frequency of $f = 0.1$ Hz. In the test with $f = 0.5$ Hz failure occurred after 802 cycles, that means after an approx. 5 times larger number of cycles than in the case of $f = 0.1$ Hz.

In experiments on tube samples, one load cycle with a loading frequency of $f = 0.01$ Hz was found to have the same effect as 1.5 to 5 load cycles with $f = 0.1$ Hz [3]. The frequency-dependence observed for the Onsøy clay block samples lays at the upper boundary of that range.

4.3 Block samples from shallower depth

Eight samples were cut out of block No. 18 which was taken from a shallower depth than the blocks Nos. 26 and 27. Consequently, the in-situ stresses are lower (σ'_v = 48.1 kPa, σ'_h = 28.8 kPa). In five tests the cyclic loading was applied at the in-situ average shear stress ($t_{a,i}/s_u^c = 0.51$, samples Nos. 29, 31, 33, 34 and 36, Table 2) while in three other tests the cycles were applied at an isotropic average stress (samples Nos. 35, 37 and 38). Amplitude ratios $t_{cy,i}/s_u^c$ between 0.30 and 0.90 were tested. A loading frequency of 0.1 Hz was used in all tests. Similar to the tests on the block samples from greater depths, the permanent strain failure mode was observed for $t_{a,i}/s_u^c = 0.51$ (Figure 11a,b) while the strain amplitude failure mode was obtained for $t_{a,i}/s_u^c = 0$ (Figure 11d,e). In Figure 11c,f the curves $t_{cy}/s_u^c(N_f)$ obtained from the tests on the samples from block No. 18 are compared to similar data for block No. 26. Obviously, the undrained cyclic strength measured for the samples from shallower depth is slightly larger, despite a lower plasticity index of the clay. This becomes also clear from Figure 6, where the isoline for $N_f = 10$ obtained from the tests on block No. 18 has been added as thick dashed curve. This isoline lies in the range of tube sample data for soils having considerably higher plasticity indices than Onsøy clay.

4.4 Influence of sample geometry

All the tests discussed so far have been performed on samples with a height-to-diameter ratio of $h/d = 2$ using rough end plates. For comparison purpose four tests were performed on samples with $h/d = 1$ using smeared end plates. These four samples (Nos. 39 to 42) were cut from the fourth layer of block No. 26. Judging by the void ratio change $\Delta e_c/e_0$ measured during re-consolidation (Table 2), these samples were more disturbed than those cut from the upper layers of block No. 26. Consequently, a lower s_u^c-value was determined in the monotonic tests (Table 1). In the four tests on the samples with $h/d = 1$, the cycles were applied at the in-situ average shear stress ($t_{a,i}/s_u^c = 0.57$), using amplitude ratios $t_{cy,i}/s_u^c$ between 0.35 and 0.65 and a loading frequency of 0.1 Hz. Similar to the samples with $h/d = 2$, also all samples with $h/d = 1$ failed due to an excessive accumulation of permanent strain, while the strain amplitude remained relatively small. Figure 12 compares the relationship $t_{cy}/s_u^c(N_f)$ measured for the samples with $h/d = 1$ with that obtained for samples with $h/d = 2$ in tests with similar average shear stresses and loading frequencies. The cyclic data for $h/d = 1$ was normalized by the s_u^c value measured in the monotonic test on a sample with $h/d = 1$. Although the shear plane pattern may be quite different in samples with $h/d = 1$ and $h/d = 2$ (e.g. [10]), there is hardly any difference between the cyclic resistance measured for both types of samples (Figure 12). Therefore, both sample geometries give a similar undrained cyclic strength in cyclic tests on clay.

5 DSS tests

One monotonic and two cyclic DSS tests were performed. All three samples with a diameter of $d = 67$ mm and a height of $h = 16$ mm were taken from the bottom of block No. 27. They were consolidated to the in situ effective vertical stress $\sigma'_{ac} = 72.1$ kPa. Based on the axial strains measured during re-consolidation (3.7 % $\leq \varepsilon_{a,c} \leq$ 4.2 %), the DSS test samples were more disturbed than most samples tested in the triaxial tests (compare the $\varepsilon_{\mathrm{vol},c}$-data in Tables 1 and 2). However, according to Lunne et al. [17] the sample quality may be still categorized as "good to fair".

An undrained shear strength of $s_u^{DSS} = 18.2$ kPa was measured in the monotonic test performed with a shearing rate of $\dot{\gamma} = 0.08$ %/min. The effective stress path is given in Figure 13a. Compared to the triaxial test results for sample No. 26 taken from the upper part of the same block, a ratio $s_u^{DSS}/s_u^c = 0.66$ is obtained, which compares well with test results for Drammen clay ($s_u^{DSS}/s_u^c = 0.64$) [5]. However, the larger disturbance of the DSS test sample should be kept in mind. If sample No. 43 taken from the bottom of block No. 26 with its higher sample disturbance is taken as a reference, the ratio is $s_u^{DSS}/s_u^c = 0.75$. These s_u^{DSS}/s_u^c-values lay within the range 0.57 - 0.78 reported by Lunne et al. [17] for tests on Onsøy clay block samples.

The two cyclic tests were performed with symmetrical cycles ($\tau_{a,i}/s_u^{DSS} = 0$) and different shear stress amplitudes ($\tau_{cy,i}/\ s_u^{DSS} = 0.5$ or 0.7, respectively). In both tests failure occurred due to large shear strain amplitudes $\gamma_{cy} > 15$ % (see the curves $\gamma(N)$ given in Figure 13b). As expected the number of cycles to failure decreased with increasing amplitude (Figure 13b,c). For comparison purpose, the curve $t/s_u^c(N_f)$ obtained from the triaxial tests with cycles applied at the in-situ average shear stress ($t_{a,i}/s_u^c$ = 0.48 - 0.52) has been added in Figure 13c. For a given shear stress amplitude ratio τ_{cy}/s_u^{DSS} or t_{cy}/s_u^c, failure was reached at a considerably higher number of cycles in the DSS tests than in the triaxial tests.

6 Summary and conclusions

A study with undrained monotonic and cyclic triaxial and DSS tests on high-quality block samples of soft marine Onsøy clay has been presented. In the cyclic triaxial tests different average shear stresses, shear stress amplitudes,

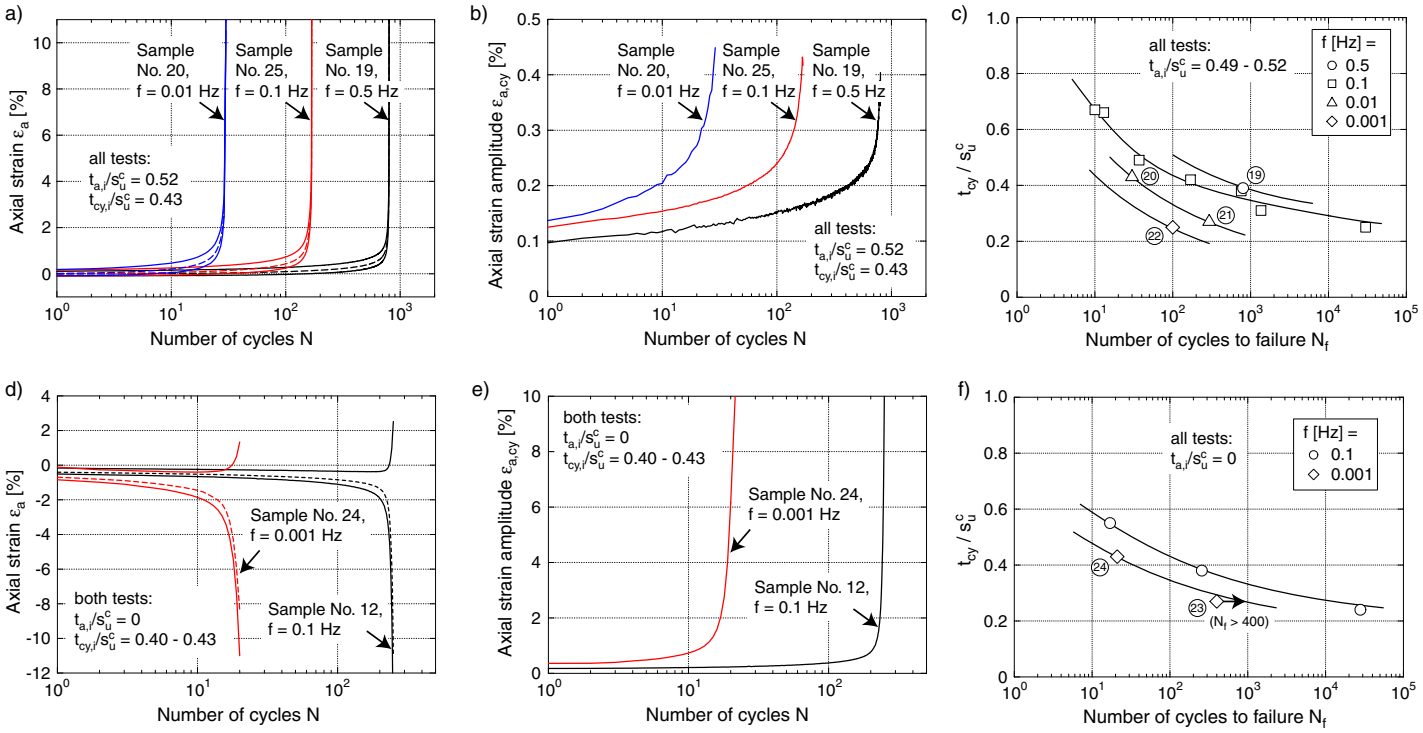

Fig. 10: *Results from tests with different loading frequencies and average stresses of a)-c) $t_{a,i}/s_u^c = 0.52$ (in-situ shear stress) and d)-f) $t_{a,i}/s_u^c = 0$ (isotropic average stress)*

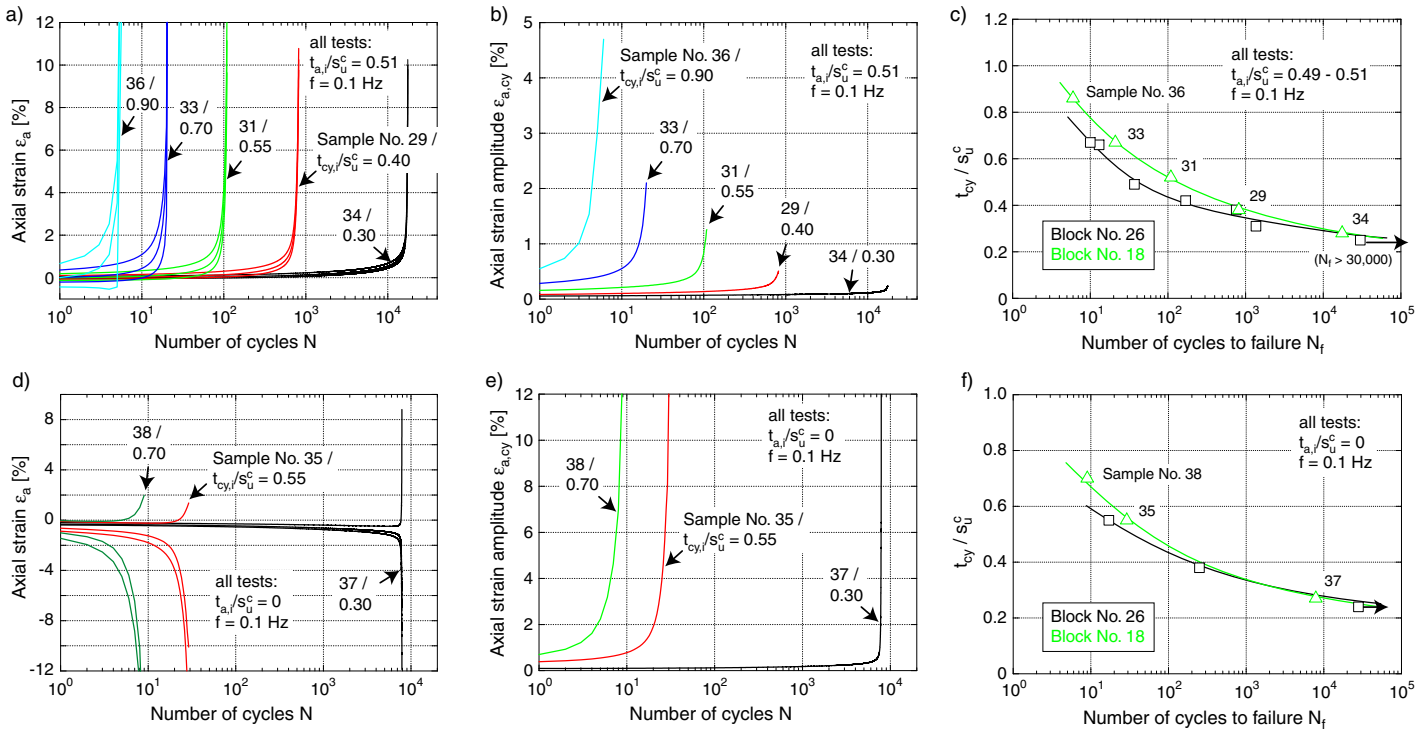

Fig. 11: *Results from tests on samples from block No. 18: a)-c) $t_{a,i}/s_u^c = 0.51$ (in-situ shear stress) and d)-f) $t_{a,i}/s_u^c = 0$ (isotropic average stress)*

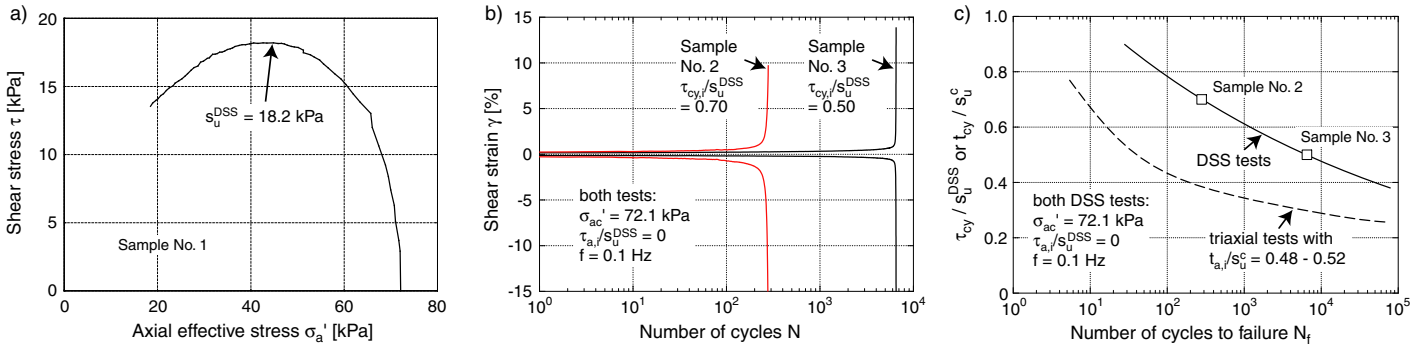

Fig. 13: *a) Effective stress path in a monotonic DSS test, b) Minimum and maximum shear strain γ as a function of the number of cycles N in two DSS tests with symmetrical cycles, c) Number of cycles to failure in dependence of amplitude ratio t_{cy}/s_u^{DSS} (for DSS test data) or t_{cy}/s_u^c (for triaxial test data)*

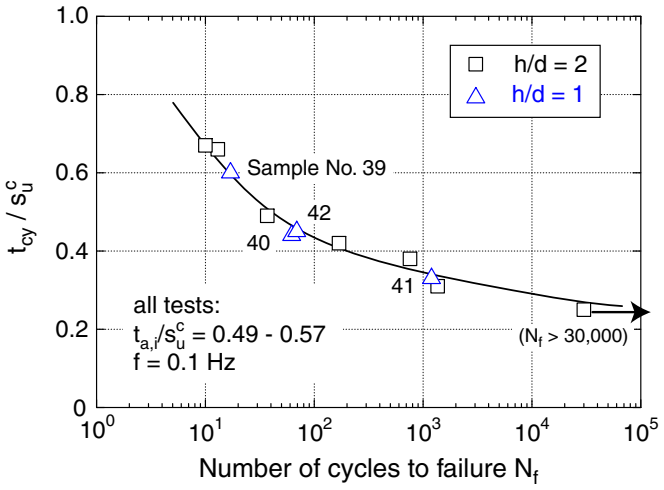

Fig. 12: *Results from tests on samples with a height-to-diameter ratio $h/d = 1$, comparison with results from tests on samples with $h/d = 2$*

loading frequencies and sample geometries have been tested on block samples obtained from different depths (approx. 7 and 11 m below ground).

In the cyclic triaxial tests the block samples failed due to large strain amplitudes for intermediate average shear stresses (in the range between $t_a/s_u^c \approx 0$ and ≈ 0.3) while a failure due to an excessive accumulation of permanent extensional or compressive strain occurred for smaller ($t_a/s_u^c < 0$) or larger average shear stress ratios ($t_a/s_u^c > 0.3$), respectively. For a given average shear stress, the number of cycles to failure decreased with increasing shear stress amplitude. Therefore, the dependence of undrained cyclic strength on average shear stress and shear stress amplitude observed for the block samples is qualitatively similar to that of standard tube samples.

Unfortunately, a direct quantitative comparison between the undrained cyclic strength of tube and block samples is not possible since cyclic data for Onsøy clay tube samples are not available yet. However, the isolines for the Onsøy clay block samples, connecting combinations of t_a/s_u^c and t_{cy}/s_u^c causing a failure in 10 cycles, have been compared with similar curves for tube samples of several other soft marine clays. The tube sample data reveals that the undrained cyclic strength tends to increase with increasing plasticity index of the clay. The undrained cyclic strength of the Onsøy clay block samples (I_P = 33 - 34 %) is considerably higher than that of Drammen clay tube samples (I_P = 27 %). It is of similar magnitude as the resistance measured for tube samples of clays having a higher plasticity index (I_P = 37 - 50 %). However, in order to quantify the possible increase of undrained cyclic strength by testing high-quality block samples instead of tube samples, tube sample data for the Onsøy clay is needed.

Based on the cyclic test data collected for the Onsøy clay block samples, diagrams have been developed which show the number of cycles to failure N_f, the permanent and amplitude values of shear strain and the permanent pore water pressure after different numbers of cycles as functions of average shear stress ratio t_a/s_u^c and shear stress amplitude ratio t_{cy}/s_u^c. These diagrams can be used for feasibility studies or for the preliminary design of foundations on clay subjected to cyclic loading.

In the tests with different frequencies, an approx. six times larger number of cycles was necessary to cause failure in the case of a frequency $f = 0.1$ Hz than in the case of a cyclic loading with $f = 0.01$ Hz. Furthermore, in a test with $f = 0.5$ Hz five times more cycles were applicable than in the case of $f = 0.1$ Hz. Compared to tube sample data, this frequency-dependence observed for the block samples is rather strong.

Block samples taken from about 7 m depth below ground showed a somewhat higher cyclic resistance than those obtained from a depth of about 11 m. In tests on samples with different height-to-diameter ratios ($h/d = 1$ and 2 were compared) no influence of the sample geometry on the normalized undrained cyclic strength could be detected. For a given shear stress amplitude ratio τ_{cy}/s_u^{DSS} or t_{cy}/s_u^c, a considerably higher number of cycles to failure was observed in the DSS tests than in the triaxial tests.

Finally, it should be mentioned that best practice tube sampling techniques using larger diameters, sharp edges and high quality stainless steel tubes may give a behavior as representative to the in situ response as block samplers. Furthermore, slower consolidation and extended aging stages may also provide improved characterization for design.

Acknowledgements

The visit of the first author at NGI was funded by German Research Council (DFG) in the framework of the project

"Behaviour of cohesive soils under high-cyclic loading: Experimental studies and constitutive description". The financial support by DFG is gratefully acknowledged herewith. All members of the NGI laboratory have contributed to this study. In particular, the help of G. Sandbækken (triaxial tests) and J. Lampe (DSS tests) is appreciated.

References

[1] K.H. Andersen. *Cyclic Loading of Soils. From Theory to Design*, chapter 4. Foundation design of offshore gravity structures.

[2] K.H. Andersen. Cyclic clay data for foundation design of structures subjected to wave loading. In T. Triantafyllidis, editor, *Cyclic Behaviour of Soils and Liquefaction Phenomena, Proc. of CBS04, Bochum*, pages 371–387. Balkema, 31 March - 02 April 2004.

[3] K.H. Andersen. Bearing capacity under cyclic loading - offshore, along the coast, and on land. The 21st Bjerrum Lecture presented in Oslo, 23 November 2007. *Canadian Geotechnical Journal*, 46(5):513–535, 2009.

[4] K.H. Andersen and K. Høeg. Deformation of soils and displacements of structures subjected to combined static and cyclic loads. In *X ECSMFE Proc., Firence*, volume 4, pages 1147–1158, 1991.

[5] K.H. Andersen, A. Kleven, and D. Heien. Cyclic Soil Data for design of gravity structures. *Journal of Geotechnical Engineering, ASCE*, 114(5):517–539, 1988.

[6] K.H. Andersen and R. Lauritzsen. Bearing Capacity for foundations with cyclic loads. *Journal of Geotechnical Engineering, ASCE*, 114(5):540–555, 1988.

[7] L.R. Bamberg. The influence of oedometer cell diameter in testing of soft clays (in Norwegian). Diploma thesis, NTNU Trondheim, 2009.

[8] T. Berre, T. Lunne, K.H. Andersen, S. Strandvik, and M. Sjursen. Potential improvements of design parameters by taking block samples of soft marine Norwegian clays. *Canadian Geotechnical Journal*, 44:698–716, 2007.

[9] E. Q. Brooker and H. O. Ireland. Earth Pressure At-Rest Related to Stress History. *Canadian Geotechnical Journal*, 2(1):1–15, 1965.

[10] J. Desrues, R. Chambon, M. Mokni, and F. Mazerolle. Void ratio evolution inside shear bands in triaxial sand specimens studied by computed tomography. *Géotechnique*, 46(3):529–546, 1996.

[11] D.W. Hight, R. Böese, A.P. Butcher, C.R.I. Clayton, and P.R. Smith. Disturbance of the Bothkennar clay prior to laboratory testing. *Géotechnique*, 42(2):199–217, 1992.

[12] D.W. Hight, A.J. Bond, and J.D. Legge. Characterization of the Bothkennar clay: an overview. *Géotechnique*, 42(2):303–347, 1992.

[13] P. La Rochelle, J. Sarrailh, F. Tavenas, M. Roy, and S. Leroueil. Causes of sampling disturbance and design of a new sampler for sensitive soils. *Canadian Geotechnical Journal*, 18(1):52–66, 1981.

[14] S. Lacasse, T. Berre, and G. Lefebvre. Block sampling of sensitive clays. In *Proceedings of the 11th International Conference on Soil Mechanics and Foundation Engineering, San Francisco, 12-16 August 1985*, pages 887–982. A.A. Balkema, Rotterdam, The Netherlands, 1985. (also published as Norwegian Geotechnical Institute Publication 163.

[15] G. Lefebvre and C. Poulin. A new method of sampling in sensitive clay. *Canadian Geotechnical Journal*, 16(1):226–233, 1979.

[16] T. Lunne and K.H. Andersen. Soft clay shear strength parameters for deepwater geotechnical design. In *Proceedings of the 6th International Conference: Society for Underwater Technology, Offshore Site Investigation and Geotechnics (SUT-OSIG), London, 11-13 September 2007*, pages 151–176, 2007.

[17] T. Lunne, T. Berre, K.H. Andersen, S. Strandvik, and M. Sjursen. Effects of sample disturbance and consolidation procedures on measured shear strength of soft marine Norwegian clays. *Canadian Geotechnical Journal*, 43:726–750, 2006.

[18] K. Yasuhara and K.H. Andersen. Recompression of normally consolidated clay after cyclic loading. *Soils and Foundations*, 31(1):83–94, 1991.

List of symbols

B	Skempton's B-value
e_0	Initial void ratio before reconsolidation
Δe_c	Void ratio change during reconsolidation
ε_a	Axial strain
$\dot{\varepsilon}_a$	Axial strain rate
$\varepsilon_{a,c}$	Axial strain during reconsolidation
$\varepsilon_{a,cy}$	Amplitude of axial strain
$\varepsilon_{a,\min}$	Minimum axial strain during a cycle
$\varepsilon_{a,\max}$	Maximum axial strain during a cycle
$\varepsilon_{a,p}$	Permanent axial strain
ε_r	Radial strain
$\varepsilon_{\mathrm{vol}}$	Volumetric strain ($= \varepsilon_1 + 2\varepsilon_3$)
$\varepsilon_{\mathrm{vol},c}$	Volumetric strain during reconsolidation
f	Frequency of cyclic loading
γ	Shear strain ($= \varepsilon_a - \varepsilon_r$ in triaxial tests)
$\dot{\gamma}$	Shear strain rate
γ_{cy}	Shear strain amplitude
γ_p	Permanent shear strain
K_0	Coefficient of earth pressure at rest
N	Number of cycles
N_f	Number of cycles to failure
OCR	Overconsolidation ratio
p	Roscoe's variable for total stresses $= (\sigma_a + 2\sigma_r)/3$
s'	Mean effective stress $= (\sigma'_a + \sigma'_r)/2$
I_P	Plasticity index
s_u	Undrained shear strength
s_u^c	Undrained shear strength in triaxial compression
s_u^e	Undrained shear strength in triaxial extension
s_u^{DSS}	Undrained shear strength from DSS tests
σ'_a	Axial effective stress
σ'_{ac}	Axial effective consolidation stress
σ'_r	Radial effective stress
σ'_{rc}	Radial effective consolidation stress
σ'_v	Vertical effective stress in situ
σ'_h	Horizontal effective stress in situ
T	Load period
t	Shear stress $= (\sigma'_a - \sigma'_r)/2$
t_{cy}	Shear stress amplitude
$t_{cy,i}$	Shear stress amplitude during first cycles
$t_{cy,f}$	Shear stress amplitude at failure
t_a	Average shear stress
$t_{a,i}$	Average shear stress during first cycles
$t_{a,f}$	Average shear stress at failure
$t_{f,cy}$	Cyclic shear strength ($= t_{a,f} + t_{cy,f}$)
t_0	Shear stress in situ
t_c	Consolidation shear stress
u_P	Permanent (excess) pore water pressure
w_c	Water content after reconsolidation
w_L	Liquid limit

w_P Plastic limit